Combinatorial effects of multiple genes contribute to beneficial aneuploidy phenotypes

M. Sophie Koller[1,2], Claudia Himmelbauer [1], Sarah Fink[1], Madhwesh C. Ravichandran[1], Christopher S. Campbell[1@]

[1]Department of Chromosome Biology, Max Perutz Labs, University of Vienna, Vienna Biocenter (VBC), A-1030 Vienna, Austria

[2]Vienna Biocenter PhD Program, a Doctoral School of the University of Vienna and the Medical University of Vienna, A-1030 Vienna, Austria

@: Christopher S. Campbell

Email: christopher.campbell@univie.ac.at

Phone: +43-1-4277-74418

Address: Dr. Bohr-Gasse 9/5, A-1030 Vienna, Austria

Keywords: Aneuploidy; complex karyotypes; drug resistance; tubulin expression;

Abstract

Aneuploidy is one of the most common adaptive mechanisms to environmental selection in cells, yet its advantages over other genomic alterations remain unclear. We used budding yeast to determine if beneficial aneuploidy phenotypes are driven primarily by combinatorial expression changes of multiple genes. To determine the impact of complex aneuploidy on cellular fitness and drug resistance, we generated yeast collections with nearly every combination of two chromosome gains or losses. Additionally, we genetically dissected aneuploid chromosomes using partial deletions to identify chromosomal regions contributing to aneuploidy-driven drug resistance. Strong resistance phenotypes consistently came from combinations of chromosomes or chromosomal regions, with up to five regions on a chromosome contributing to resistance to a single drug. Gene ontology terms had limited predictive power in identifying the genes contributing to resistance phenotypes, as the combinatorial effects from different aneuploid regions act through multiple resistance pathways. The strongest phenotypes came from synergistic effects between copy number changes of different chromosomes or chromosomal regions, demonstrating how subtle gene expression changes of many genes combine to greatly impact cell survival.

Introduction

The accurate distribution of chromosomes during cell division is essential for maintaining genomic integrity across all eukaryotic species. Chromosome segregation errors result in alterations in chromosome copy number, which are termed aneuploidy. Aneuploidy is one of the most common genetic alterations in cancer, occurring in ~90% of solid tumors and ~70% of hematopoietic cancers (Weaver and Cleveland 2006). These high frequencies of aneuploidy are not only inherent to cancer cells but are also commonly observed within other vegetatively growing cell populations including industrial strains of baker's yeast and drug resistant strains of the human pathogens *Candida albicans* and *Leishmania* (Selmecki et al. 2006; Ubeda et al. 2008; Peter et al. 2018; Loegler et al. 2024).

Despite the frequency of aneuploidy in mitotically growing cell populations, it is generally associated with reduced cellular fitness. Engineering aneuploidy in cells invariably decreases growth rates under optimal conditions (Torres et al. 2007; Stingele et al. 2012; Hintzen et al. 2022; Zerbib et al. 2024). This decrease in fitness results from changes in gene copy numbers of many transcribed genes on the aneuploid chromosome (Bonney et al. 2015). For both yeast and human cells, gene expression levels of lab engineered aneuploidies scale with gene copy numbers for most of the aneuploid genes (Torres et al. 2007; Stingele et al. 2012; Wangsa et al. 2019; Rojas et al. 2024; Muenzner et al. 2024). These small changes in expression levels for hundreds of genes cause a wide range of deleterious phenotypes. Such general aneuploidy-associated phenotypes include increased proteotoxic stress, cell cycle delays, and increased DNA damage (Torres et al. 2007; Sheltzer et al. 2011; Thorburn et al. 2013; Oromendia et al. 2012; Beach et al. 2017; Li and Zhu 2022; Williams et al. 2008; Passerini et al. 2016; Santaguida et al. 2015; Garribba et al. 2023).

Yet, aneuploidy is one of the most frequently observed mechanisms of cellular adaptation. The first direct link between adaptive drug resistance and aneuploidy was established in the human pathogen *Candida albicans* (Selmecki et al. 2006). Adaptation via aneuploidy has since been more extensively observed in the budding yeast *Saccharomyces cerevisiae,* where specific aneuploidies consistently emerge

during experimental evolution screens under adverse environmental conditions (Gresham et al. 2008; Yona et al. 2012; Chen et al. 2012; Voordeckers et al. 2015; Zhang et al. 2016; Beaupere et al. 2018; Morard et al. 2019). Moreover, inducing aneuploidy via random chromosome missegregation in both yeast and human cells promotes resistance to a large variety of drugs (Pavelka et al. 2010; Chen et al. 2012; Lukow et al. 2021; Ippolito et al. 2021). Aneuploidy can also act as a suppressor of mutations that decrease cellular fitness (Rancati et al. 2008; Liu et al. 2015; Ryu et al. 2016; Ravichandran et al. 2018; Macaluso et al. 2025). In cancer, karyotype patterns have predictive power for drug resistance, tumor progression and patient outcome (Shukla et al. 2020).

The potential for aneuploidy as an adaptation mechanism to a large variety of selective environments can partially explain the high prevalence of aneuploidy following long-term vegetative growth, such as in cancer or in yeast used for alcohol production (Peter et al. 2018). However, it still fails to explain why cells adapt through aneuploidy over other types of mutations that don't share its inherent downsides. Different models for the specific advantage of adaptation through aneuploidy have been proposed. Aneuploidy has been suggested to be a rapid, but transient solution to sudden environmental changes. In *S. cerevisiae* subjected to acute heat stress, chromosome 3 is gained early in the adaptation process but then lost again over time (Yona et al. 2012). Similarly, yeast adapting to high rates of chromosomal instability (CIN) adapted first through the accumulation of specific aneuploidies, followed later by the accumulation of suppressor point mutations (Clarke et al. 2023). However, there are also many examples of specific aneuploidies that are maintained throughout long-term adaptation, highlighting that speed is likely not the only advantage of adaptation via aneuploidy (Selmecki et al. 2009; Ravichandran et al. 2018; Adell et al. 2023; Clarke et al. 2023; Zhou et al. 2024; Watson et al. 2024).

An additional explanation for the advantages of aneuploidy as a mechanism of adaptation comes from its ability to change gene expression levels of several beneficial genes simultaneously. In yeast adaptation screens, only a handful of examples could attribute the selective advantage of aneuploidy to changes in expression levels of one or two specific genes. Even in these cases, they rarely recapitulated the strength of the aneuploidy phenotype (Selmecki et al. 2009; Chen et

al. 2012; Ryu et al. 2016; Linder et al. 2017; Beaupere et al. 2018; Ravichandran et al. 2018; Barney et al. 2021; Pavani et al. 2021; Zhou et al. 2024). In cancer, overexpression of individual genes also fails to fully recapitulate the phenotypes of aneuploid chromosomes (Trakala et al. 2021; Su et al. 2021; Girish et al. 2023). These findings suggest that the challenges of identifying driver genes on aneuploid chromosomes could be amplified by the interplay between multiple genes. It is currently unclear how many genes on aneuploid chromosomes typically contribute to the resistance to selective pressures.

Analyses of aneuploidy patterns in cancer genomes as well as cellular adaptation experiments have shown strong correlations between specific chromosome or chromosome arm combinations, indicating karyotype selection is influenced by genetic interactions between aneuploid chromosomes (Ozery-Flato et al. 2011; Ravichandran et al. 2018; Shukla et al. 2020; Adell et al. 2023). One such interaction has been observed in budding yeast, where gaining an additional copy of chromosome 6 is lethal, but can be rescued with the additional gain of chromosome 13 (Torres et al. 2007). Whether such genetic interactions between chromosome are widespread is currently unknown. An alternative explanation for karyotype pattern formation is that selective pressure could enrich for sets of beneficial aneuploidies, either independently or through selection-specific chromosomal genetic interactions.

In this study, we generated a large yeast collection with nearly every possible combination of two chromosome gains or losses to determine the frequency and strength of genetic interactions between aneuploid chromosomes and how combinatorial aneuploidy phenotypes impact drug resistance and sensitivity. We found that genetic interactions between chromosomes are rare in the absence of treatment but become much more frequent under strong selective pressure. In addition, the strongest resistance phenotypes consistently came from combinations of aneuploid chromosomes, demonstrating the advantage of copy number changes in multiple genes. We genetically dissected resistant aneuploid chromosomes using partial arm deletions to determine the number of regions that contribute to aneuploidy-driven drug resistance on a single chromosome. We found that resistance conferred by single disomies nearly always comes from multiple chromosomal regions. While the majority

119 of phenotypes are additive, the strongest resistance phenotypes of aneuploidies came
120 from synergistic effects between different regions or chromosomes.
121

122 **Results**

123 **Generation of yeast strain libraries with combinations of chromosome gains**
124 **and losses**

125 We first determined how aneuploidy of different regions of the genome combine to
126 impact cellular fitness and drug response by generating two collections of yeast with
127 combinations of chromosome gains or losses. The collections consist of nearly all
128 possible single and double chromosome gains and losses (Fig 1A). To engineer
129 chromosome gain or loss, chromosome-specific missegregation was first induced via
130 a strong galactose-inducible centromere-proximal promotor, followed by selection for
131 the specific aneuploidy (Fig S1A). We selected for chromosome gains via
132 recombination events that restore the function of an auxotrophic marker. Chromosome
133 loss was generated by selecting against the *URA3* gene using 5-fluoroorotic acid (5-
134 FOA) (Fig S1A). The chromosome gain collection includes most of the possible single
135 (14/16) and double disomic (90/136) strains in haploid cells; each was confirmed by
136 qPCR (Table S1). The chromosome loss collection contains every possible single or
137 double monosomy in diploid cells (Fig S1B). Since chromosome loss cannot be
138 continuously selected for, this collection is inducible to generate newly aneuploid cells
139 prior to each experiment. These libraries currently constitute the largest collections of
140 engineered complex aneuploid cells.
141

142 We first evaluated the libraries by measuring the growth rates of the engineered
143 aneuploidy strains under optimal growth conditions. The high-throughput growth rate
144 measurements of single disomies and monosomies strongly correlate with those
145 previously observed (Beach et al. 2017) (Fig S1C). The previously published
146 measurements were performed in a strain background containing a mutation in the
147 *SSD1* gene, which has been reported to sensitize cells to aneuploidy phenotypes
148 (Hose et al. 2020). However, we observe similar results in a different, wildtype *SSD1*
149 background (S288c), indicating that strain background does not substantially alter the
150 relative growth rate of aneuploid yeast. The ability to reproduce the previously

published correlations between gene number and phenotypic strength and the differences between chromosome gain and loss attest to the quality of these strain collections.

We next determined the impact of combining aneuploid chromosomes on cellular fitness. Growth of complex aneuploidies negatively correlated with the number of open reading frames (ORFs) on the aneuploid chromosomes for both chromosome gain and loss (Fig 1B). While most of the single and double monosomies are lethal, nearly all of the double disomies are viable, with the sole exception of those involving chromosome 6 (Fig 1B and Fig S1B). The strongest outlier is the combination of chromosomes 6 and 13 (Fig 1C). Chromosome 6 disomy is lethal on its own due to the presence of an extra copy of the β-tubulin *TUB2* gene (Anders et al. 2009). However, chromosome 6 disomy becomes viable with the additional gain of chromosome 13. This is consistent with previous observations where selection of chromosome 6 gain resulted in a strain that spontaneously gained the additional disomies of chromosomes 1 and 13 (Torres et al. 2007). Chromosome 13 contains the genes for α-tubulin, and overexpression of α-tubulin rescues the lethality of chromosome 6 disomy (Anders et al. 2009). For the chromosome loss collection, one of the strongest genetic interactions is again between chromosomes 6 and 13 (Fig. 1D). Chromosome 13 monosomy is lethal on its own, but the additional loss of chromosome 6 rescues viability (Fig 1D). The heterozygous deletion of *TUB2* is sufficient to rescue chromosome 13 monosomy, indicating that excess β-tubulin relative to α-tubulin is the genetic basis behind these strong chromosome copy number interactions (Fig 1D).

To identify any additional genetic interaction between chromosome gains, we calculated growth predictions for all chromosome combinations based on the product of the growth of the individual single aneuploidies. In general, growth of the double disomies correlates well ($r^2 = 0.64$) with the calculated growth predictions (Fig 1C). To measure genetic interaction between aneuploid chromosomes, we calculated an epistasis score by subtracting predicted growth from the measured growth of the chromosome combinations. The epistasis scores strongly adhered to a normal distribution (Kolmogorov-Smirnov test), indicating that most combinations do not

184 deviate substantially from the expected growth rate (Fig S1D). Among the 90
185 chromosome combinations analyzed, we identified only 3 positive (z-score > 2) and 2
186 negative (z-score < -2) chromosome copy number interactions (Fig S1D). We
187 conclude that most combinations of aneuploid chromosomes show additive
188 phenotypes and that synergistic interactions are rare in the absence of selective
189 pressure.

190 **The strongest drug resistance phenotypes come from strains with multiple**
191 **aneuploid chromosomes**

192 We next used the chromosome gain library to determine if combinatorial interactions
193 between aneuploid chromosomes contribute to improved growth in stress conditions.
194 We measured growth in the presence of four drugs that induce cellular stresses
195 associated with aneuploidy: hygromycin B (ribosome inhibitor), rapamycin (TOR
196 pathway inhibitor), methyl methanesulfonate (MMS, DNA damage inducer) and
197 benomyl (microtubule depolymerizer) (Fig 2A). Although resistance mechanisms for
198 these drugs have been studied extensively, we aimed to identify how drug resistance
199 could be obtained by combining copy number changes of multiple regions in the
200 genome. Drug concentrations were titrated to reduce wild-type growth by ~80%.
201 Growth was unaffected by the solvent used to resuspend the drugs (Fig S1E).
202 Aneuploidy substantially altered the cellular response to hygromycin, rapamycin, and
203 benomyl, as growth rates no longer scaled with number of genes on aneuploid
204 chromosomes (Fig 2B). By contrast, MMS treatment showed fewer aneuploidy-
205 associated phenotypes. The percentage of strains displaying substantial relative
206 resistance (normalized growth in the presence/absence of the drug > 2) across the
207 entire library varies greatly between the different drugs ranging from 59% for benomyl
208 to 9% for MMS (Fig S2B and C). We conclude that the capacity for aneuploidy to
209 provide resistance is drug dependent.
210
211 In addition to drug resistance, we also observed frequent drug sensitivity. This was
212 most pronounced for hygromycin, where over 78% of strains showed a greater than
213 two-fold relative decrease in growth in the presence of the drug (Fig S2B). Additionally,
214 we measured sensitivity to two stress conditions other than drugs: 39°C for heat stress
215 and 18°C for cold stress. Neither of these conditions greatly influenced cell growth in

216 the euploid strain. However, heat stress led to a two-fold decrease in growth for 66%
217 of the disomic strains, which scaled with the degree of aneuploidy (Fig S2A-C). These
218 results suggest that aneuploid yeast are especially sensitive to hygromycin and heat
219 stress, which implicate translation inhibition and protein misfolding as potential
220 vulnerabilities in aneuploid cells. This would agree with previous reports that aneuploid
221 strains frequently exhibit decreased ribosome levels and proteotoxic stress
222 (Oromendia et al. 2012; Terhorst et al. 2020).
223
224 We next wanted to determine if combinations of aneuploid chromosomes show
225 stronger phenotypes than individual chromosomes. For hygromycin, rapamycin and
226 benomyl, specific chromosome combinations had the highest levels of drug
227 resistance, despite their negative impact on fitness in the absence of the drugs
228 (Fig 2C). Notably, absolute resistance to hygromycin was observed only for
229 chromosome combinations, as none of the single disomies grew better than the
230 euploid strain in the presence of hygromycin. We measured genetic interactions
231 between chromosomes in the same manner as for the untreated cells by comparing
232 the growth of the chromosome combinations to the predicted growth based on the
233 single disomies. For all four drugs, the epistasis scores no longer fit a normal
234 distribution, suggesting more frequent deviations from the predicted growth (Fig. S2E).
235 Indeed, after using the same threshold for epistasis scores as we applied to the
236 untreated condition, there were substantially more positive and negative genetic
237 interactions following drug treatment as compared to untreated cells (Fig 2D). Overall,
238 we conclude that the strongest drug resistance aneuploidy phenotypes typically come
239 from the combined effects of multiple genes on different chromosomes and that
240 selective pressure increases the frequency of chromosome copy number interactions.
241
242 **Benomyl resistance correlates with α-Tubulin expression in aneuploid strains.**
243 Surprisingly, a majority (59%) of disomic chromosome combinations were resistant to
244 the microtubule depolymerizing factor benomyl (Fig S2B and C). This high percentage
245 results from 6 of the 14 tested single disomic chromosomes conferring substantial
246 resistance to benomyl (Fig 2C and 3A). Although it has previously been reported that
247 many disomies lead to benomyl sensitivity (Sheltzer et al. 2011; Torres et al. 2007),
248 the resistance appears to outweigh the sensitivity for most chromosome combinations.
249 Benomyl resistance is therefore not a “general” aneuploidy phenotype but is instead

250 karyotype specific, despite being observed in the majority of double disomic strains.
251 Aneuploidy frequently leading to resistance to microtubule inhibitors was not specific
252 to benomyl, as four of the same aneuploid chromosomes provided resistance to
253 another microtubule depolymerizing drug, nocodazole (Fig S3A). We first focused on
254 chromosome 13, as it contains both α-tubulin genes (*TUB1* and *TUB3*) and α-tubulin
255 overexpression has been shown to result in a mild increase in benomyl resistance
256 (Schatz et al. 1986). Heterozygous deletion of *TUB3* in the chromosome 13 disomic
257 strain eliminated the resistance phenotype, demonstrating the contribution of this gene
258 to the resistance (Fig S3B). To determine if α-tubulin protein abundance contributes to
259 benomyl resistance in the other aneuploid strains, we measured the expression levels
260 in all 14 disomic strains via quantitative western blots. We found that multiple single
261 disomies alter α-tubulin expression levels (Fig 3B). The measured α-tubulin
262 expression levels correlated well with those measured by proteomics of aneuploid
263 yeast strains, demonstrating that these differences occur independently of the
264 measurement method and strain background (Fig S3C and D; (Muenzner et al. 2024;
265 Dephoure et al. 2014)). Elevated α-tubulin expression levels strongly correlated with
266 the degree of benomyl resistance for the single disomies, suggesting that this is a
267 major mechanism of resistance (Fig 3C and Fig S3E). Intriguingly, only chromosome
268 12 disomy is extremely sensitive to benomyl and is also the only disomy that shows a
269 substantial decrease in α-tubulin expression. The correlation with benomyl resistance
270 was much weaker for β-tubulin expression (Fig 3C, Fig S3F and G). These results
271 demonstrate that there are multiple genes across the genome that can alter tubulin
272 expression levels when present at an extra copy, and that these mild expression
273 changes can greatly alter the response to microtubule inhibitors.
274
275 To identify candidate resistance genes on the aneuploidy chromosomes, we started
276 by looking at gene ontology (GO) terms associated with the molecular target (tubulin),
277 associated phenotype (CIN), and drug sensitivity screens of the yeast deletion
278 collection. None of these terms showed a significant enrichment on the resistant
279 aneuploid chromosomes (Fig S4A). Furthermore, there were between 64 and 195
280 candidate genes per chromosome identified this way (Fig S4B). To further refine the
281 list of candidate genes, we focused on genes with substantial increases in RNA and
282 protein levels on the aneuploid chromosomes (Torres et al. 2007; and Dephoure et al.

2014). Applying an overexpression threshold of 1.5-fold for candidate proteins only reduced the list by 32%. We therefore sought to identify chromosomal regions responsible for drug resistance to decrease the number of candidate resistance genes.

Identification of chromosome arms necessary for aneuploidy-based drug resistance.

We next aimed to determine which regions of particular chromosomes provide resistance when gained by a single copy. We focused primarily on benomyl resistance, since six individual disomies led to strong resistance to the drug. This provided multiple examples to systematically examine how many regions/genes typically contribute to positive aneuploidy phenotypes for single aneuploid chromosomes. One possibility is that a single strong resistance gene on each chromosome could be sufficient to give a substantial fitness advantage under harsh drug conditions (single gene model). Another possibility is that multiple mildly beneficial genes on single chromosomes may act together to create strong resistance phenotypes (combinatorial model) (Fig 4A).

To determine which regions of chromosomes have negative, positive, or neutral effects on growth with and without benomyl, we implemented a method that deletes part of a chromosome from the end and replaces it with a selection marker and an artificial telomere (Linder et al., 2017) (Fig 4B). We first generated single arm disomies of all of the benomyl resistant single disomic chromosomes. The deletion of one of the two copies of the chromosome arms was confirmed by qPCR. As with whole chromosome disomies, arm-level disomies have decreased growth rates proportional to the number of aneuploid ORFs under standard conditions (Fig 4C). Benomyl resistance was frequently associated with a single arm. For chromosomes 2, 4, 10, and 14, disomy of the larger arm was sufficient to fully recapitulate the benomyl resistance, whereas chromosome 13 only showed resistance with disomy of the shorter arm (Fig 4D). Both α-tubulin genes (*TUB1 and TUB3)* are on the short (left) arm of chromosome 13. Intriguingly, neither of the chromosome 5 arm disomies recapitulated the benomyl resistance of the whole chromosome disomy. Chromosome 5 left arm disomy shows no resistance, while the right arm disomy is only mildly resistant. Therefore, the benomyl resistance for chromosome 5 results from at least one gene on each of the

317 two chromosome arms (Fig 4D). Overall, the correlation between growth with and
318 without benomyl for the arm-level disomies was not significant, demonstrating that
319 benomyl resistance is not the result of slow growth or a general aneuploidy phenotype
320 (Fig S5A). Instead, resistance likely results from the increased expression of one or
321 more specific genes on the aneuploid chromosome arms.
322
323 Next, we used our arm level aneuploidies to analyze resistance or sensitivity to the
324 three other drugs tested: hygromycin, MMS and rapamycin (Fig S6B). Similar to
325 benomyl, resistance to MMS, rapamycin and hygromycin was primarily associated
326 with single chromosome arms (3/3). By contrast, arm-level aneuploidies generally did
327 not fully recapitulate increased drug sensitivity phenotypes (Fig 4E and Fig S5B and
328 C). Instead, both arms often showed partial sensitivity. This is also the case for the
329 only chromosome that showed strong sensitivity to benomyl, chromosome 12 (Fig 4D).
330 These results suggest that aneuploidy-based drug sensitivity results from the
331 combined effects of more genes than drug resistance. Surprisingly, in some examples,
332 drug sensitivity from one chromosome arm was compensated for by the resistance
333 from the second chromosome arm (2/8) (Fig S5B and C).

334 **Most aneuploidy-based drug resistance phenotypes come from the combined**
335 **effect of multiple genes**

336 Since most of the resistance phenotypes were associated with the larger arms, we
337 wanted to determine how many regions/genes on these arms contribute to benomyl
338 resistance. We therefore made multiple shorter deletions to the benomyl resistant
339 disomies to identify regions of drug resistance. For example, seven additional cuts
340 were made on the right arm of chromosome 4 to identify regions of interest. As the
341 size of the chromosome decreased, growth under standard conditions gradually
342 increased (Fig 5A). This further demonstrates that the negative effects on fitness for
343 aneuploid strains result from many genes across the length of a chromosome (Bonney
344 et al. 2015). Conversely, benomyl resistance decreased in a stepwise manner
345 following the deletion of three independent regions on the right arm (Fig 5A). For 5 of
346 the 6 resistant chromosomes, we identified at least two regions that contributed to
347 resistance, with the most being 5 regions for chromosome 5 (Fig 5C and Fig. S6A).
348 Interestingly, three of the benomyl resistant chromosomes also had regions that

349 increased drug sensitivity (Fig 5A and C and Fig S6A). The strength of drug resistance
350 is therefore a balance between regions that confer resistance and sensitivity.
351
352 To determine if the regions that lead to benomyl resistance also increase α-tubulin
353 protein levels, we examined the segmental deletions of chromosome 5 in the disomic
354 strain. Despite both arms of chromosome 5 contributing to benomyl resistance, only
355 the right arm was necessary for the increased α-tubulin levels. Removal of a single
356 region on the right arm decreased the α-tubulin levels back to euploid levels (Fig S5B).
357 The identified 60kb region also contributes to benomyl resistance. This region does
358 not contain any genes with an associated tubulin/microtubule gene ontology term.
359 None of the other 4 resistance regions contributing to benomyl resistance impacted α-
360 tubulin protein levels, indicating that these regions confer benomyl resistance through
361 alternative mechanisms.
362
363 We next aimed to identify the resistance genes within the identified regions. The
364 regions each contain between ~30 and 100 genes. We identified candidate genes by
365 looking for: sensitivity to benomyl in high-throughput screens of the yeast knockout
366 collection, essential genes, and genes that have GO Terms associated with CIN and
367 tubulin/microtubules (Fig S4B). Candidate genes were tested via heterozygous
368 deletions in the disomic strains (Fig S7A). For the two regions on chromosome 4
369 associated with the strongest benomyl resistance, we identified single gene deletions
370 that decreased resistance to a similar extent as deleting the entire chromosomal
371 region (Fig 5B and C). In total, we identified 9 genes that decrease the resistance of
372 aneuploid chromosomes when deleted heterozygously (Fig S7A and S8). In addition
373 to *TUB3* on chromosome 13, we identified two additional genes associated with tubulin
374 (*GIM4*-chr.5, *PFD1*-chr.10). Both of these genes are members of the prefoldin
375 complex, which is a chaperone that promotes the proper folding and assembly of α-
376 and β-tubulin. One resistance gene is involved in microtubule stabilization (*BIM1*-
377 chr.5). Interestingly, two of the resistance genes have recently been implicated in the
378 spindle position checkpoint (*SWR1*-chr.4, *MCK1*-chr.14) (Rathi et al. 2022; Caydasi et
379 al. 2023). Another resistance gene, *TOF1*-chr.14, is primarily associated with
380 protection of the DNA replication fork. However, it shows a synthetic lethal interaction
381 with *BIM1*, indicating an additional role in chromosome segregation (Tong et al. 2004;

382 Pan et al. 2004). Overall, we have identified many genes across the genome with a
383 variety of different functions that contribute to aneuploidy-based benomyl resistance.
384
385 Previous studies have only identified two or three genes responsible for resistance
386 phenotypes for individual perturbations, prohibiting any significant analysis of the
387 characteristics of genes that can contribute to aneuploidy phenotypes either in yeast
388 (rev. in Tsai and Nelliat 2019) or human cells (Adell et al. 2023; Ippolito et al. 2021).
389 We assessed whether the 9 genes identified shared common features using GO
390 enrichment, RNA expression levels and protein abundance. Intriguingly, GO
391 overrepresentation analysis of the nine identified benomyl resistance genes did not
392 reveal any significant enrichment terms as measured by adjusted p-values (Fig S7D).
393 In addition, the highest ranked hit, “microtubule cytoskeleton organization”, only
394 contained 3 out of 9 genes. This highlights the diversity of gene functions that can
395 combine to contribute to aneuploidy-based drug resistance.
396
397 Different genes can have substantial differences in the degree to which their
398 expression increases when an additional copy is gained on an aneuploid chromosome
399 (Stingele et al. 2012; Dephoure et al. 2014; Muenzner et al. 2024; Hwang et al. 2021;
400 Sousa et al. 2019). We therefore hypothesized that genes that contribute to beneficial
401 aneuploidy phenotypes would be those that have their expression levels more
402 substantially altered by aneuploidy. Analysis of the increase in RNA expression levels
403 for genes on aneuploid chromosomes showed a small, yet significant increase for the
404 9 benomyl resistance genes when compared to the rest of the genes on these
405 chromosomes (Torres et al. 2007; Fig S7E) However, this may reflect a bias in the
406 selection of candidate genes, as there was no significant difference between the tested
407 genes that either did or did not contribute to benomyl resistance (Fig S7F). For the 7
408 benomyl resistance genes where increased protein levels on aneuploid chromosomes
409 have been measured, there were no significant differences in expression levels (Fig
410 S7E and F). We conclude that genes affecting aneuploidy phenotypes are not
411 enriched for genes with more substantial increases in expression on aneuploid
412 chromosomes.
413
414 In addition to the disomic chromosomes that lead to benomyl resistance, we also
415 identified chromosomal regions that lead to rapamycin resistance on chromosome 10.

416 Strains with disomy of chromosome 10 have previously been shown to be rapamycin
417 resistant (Torres et al. 2007). This was speculated to be due to the presence of the
418 *TOR1* gene. Heterozygous deletion of *TOR1* in a chromosome 10 disomic strain only
419 partially decreased rapamycin resistance, indicating that there are more genes on
420 chromosome 10 that contribute to the phenotype (Fig S7B). Furthermore, both
421 chromosome arms contribute to rapamycin resistance (Fig S7C). We conclude that
422 the combined overexpression of multiple genes leading to strong phenotypes is a
423 common feature of aneuploidy.

424 **The strongest aneuploidy phenotypes result from synergistic effects**

425 Chromosome 5 disomy has the strongest benomyl resistance phenotype and is the
426 only chromosome where both arms contribute to the phenotype (Fig 4D). Additionally,
427 the degree of resistance for the whole chromosome was substantially higher than
428 either of the two individual arm-level disomies, suggesting a synergistic interaction
429 between the two arms. To look at this more systematically, we predicted the strength
430 of resistance for whole chromosome aneuploidy based on the resistance of the
431 individual arm-level aneuploidies (Fig 6A). Although the other single disomies
432 displayed resistance in line with the predictions, benomyl resistance for chromosome
433 5 was substantially higher than predicted. This demonstrates a strong synergistic
434 interaction between the two arms.
435
436 We next wanted to determine if the strongest phenotypes for double disomic strains
437 also result from synergistic interactions. We focused on chromosome combinations
438 where the single disomies on their own were benomyl resistant. We initially observed
439 that the combined disomies of chromosomes 2 & 4 and 2 & 13 are exceptionally
440 strong, showing robust resistance even at higher benomyl concentrations (Fig 6B).
441 These combinations are as resistant as a deletion mutation known to be highly
442 resistant to benomyl (Schibler et al. 2016), despite strong growth defects for aneuploid
443 strains in the absence of the drug (Fig 6C). These high levels of resistance do not
444 result from further increases in α-tubulin expression levels (Fig S9A). Looking at
445 combinations with chromosome 2 specifically, we observed a wide range of resistance
446 phenotypes, ranging from strong positive to strong negative interactions (Fig 6B and
447 Fig S9B). Strikingly, a strong negative genetic interaction between chromosomes 2

and 14 results in the near-complete loss of the benomyl resistance (Fig 6B and D). Almost all combinations with chromosome 14 grow worse than the single disomies (Fig S9C), indicating a general negative effect of chromosome 14 combinations and benomyl resistance. We also observed a positive synergistic interaction between chromosomes 3 and 12 for rapamycin resistance, demonstrating that such strong genetic interactions are not benomyl-specific (Fig S9D). We conclude that most aneuploidies display additive effects between genes, regions, and chromosomes. However, the strongest beneficial growth phenotypes often come from synergistic interactions.

Discussion

In this study, we generated a library of engineered single and double aneuploid yeast strains to systematically determine the genetic drivers of aneuploidy-based drug resistance. In addition, we used a comprehensive approach to identify regions/genes on aneuploid chromosomes that contribute to aneuploidy phenotypes. This approach has numerous advantages, allowing for the identification of: i) multiple regions on a chromosome that contribute to a phenotype, ii) both resistant and sensitive regions on a single chromosome, iii) regions that act synergistically, where each region on its own would not have a strong phenotype. Together, these strategies provide a means to comprehensively identify the genetic determinants of positive and negative selection for aneuploid chromosomes either alone or in combination.

When measuring the resistance of the chromosome gain collection to four different inhibitors, the strongest resistance phenotypes were consistently identified for chromosome combinations. This demonstrates that altered copy numbers of multiple genes combine to create stronger beneficial aneuploidy phenotypes. These additional benefits are observed despite the often substantial negative growth phenotypes for the double aneuploid strains under optimal growth conditions. Therefore, the benefits of combining multiple aneuploid chromosomes generally outweigh the downsides under selective conditions. Furthermore, we saw these positive combinatorial effects for 3 of the 4 drug conditions, suggesting that it is a general property of aneuploidy. This combinatorial behavior of aneuploid chromosomes could explain the frequent occurrence of complex aneuploidy in both adapted yeast populations and cancer

482 karyotypes (Mitelman Database of Chromosome Aberrations and Gene Fusions in
483 Cancer, 2025. https://mitelmandatabase.isb-cgc.org, (Rancati et al. 2008;
484 Ravichandran et al. 2018; Peter et al. 2018; Klockner and Campbell 2024).
485
486 In addition to identifying strong phenotypes for combinations of aneuploid
487 chromosomes, we discovered multiple regions within individual chromosomes that
488 contribute to drug resistance phenotypes. We identified up to 5 regions on a single
489 chromosome that contribute to drug resistance, emphasizing that multiple genes are
490 typically responsible for strong aneuploidy phenotypes. This combinatorial action of
491 many genes suggests an advantage for the selection of aneuploidy over other types
492 of genomic alterations. Changing the expression of genes with distinct and
493 complementary functions may provide proliferative benefits that could not be
494 accomplished through single mutations. These data provide substantial support for a
495 “combinatorial genes” explanation for the specific benefits of aneuploidy over other
496 genomic alterations.
497
498 In the absence of selection, we did not observed strong genetic interactions between
499 chromosome gains with the exception of the combination of chromosomes 6 and 13.
500 However, it is worth noting that even relatively weak interactions have the potential to
501 affect aneuploidy patterns (Ravichandran et al. 2018). By contrast, under selection,
502 the number of genetic interactions between chromosomes was substantially increased
503 for all 4 of the drugs tested. Furthermore, increasing the degree of selection via higher
504 concentrations of benomyl revealed strong positive synergistic interactions between
505 aneuploid chromosomes. We also observed a clear synergistic interaction between
506 the arms of chromosome 5. These results suggest another possible advantage for
507 adaptation through aneuploidy, wherein the altered expression levels of two
508 complementary genes would not be selected for individually due to a lack of
509 phenotype. However, two simultaneous changes to the genome through a single
510 chromosome missegregation event would enable their combined selection, leading to
511 a strong beneficial phenotype. These results, along with the recently discovered
512 synergistic interaction between chromosomes 3 and 6 in multi-azole tolerance of the
513 human pathogen *Candida albicans* (Zhou et al. 2024), demonstrate that positive
514 synergistic interactions are more heavily selected for under higher stress conditions.
515 We also find that combining beneficial aneuploidies can occasionally lead to weaker

516 than expected phenotypes, highlighting that negative genetic interactions also likely
517 impact complex karyotype formation. In cancers, positive and negative genetic
518 interactions between co-occurring aneuploidies have been suggested based on
519 correlations between chromosome arm frequencies in aneuploidy patterns (Ozery-
520 Flato et al. 2011; Ravichandran et al. 2018). Such co-occurrence patterns can be
521 highly predictive of disease progression and chemotherapy resistance in cancer
522 (Shukla et al. 2020). Our results suggest that these patterns are more likely to result
523 from specific selective pressures, rather than more general synergies or
524 incompatibilities between the gain or loss of specific chromosomes arms.
525
526 The main drivers of beneficial aneuploidy phenotypes are alterations in expression
527 levels resulting from gene copy number changes of specific resistance-driving genes
528 (Selmecki et al. 2009; Chen et al. 2012; Ryu et al. 2016; Linder et al. 2017; Beaupere
529 et al. 2018; Ravichandran et al. 2018; Barney et al. 2021; Pavani et al. 2021; Adell et
530 al. 2023; Zhou et al. 2024; Watson et al. 2024). We observed a significant correlation
531 between growth on benomyl and altered α-tubulin expression levels. In addition to
532 *TUB3* on chromosome 13, two members of the prefoldin complex (*GIM4*-chr. 5, *PFD1*-
533 chr. 10) contribute to aneuploidy-based benomyl resistance. Intriguingly, chromosome
534 12 disomy decreases tubulin expression levels and is very sensitive to microtubule
535 destabilization via benomyl. This decrease in tubulin levels for chromosome 12 disomy
536 could also help explain how it rescues microtubule hyperstabilization (Macaluso et al.
537 2025). We conclude that tubulin expression levels are not tightly regulated in yeast.
538 Furthermore, even relatively small changes in α-tubulin expression levels can
539 substantially influence resistance and sensitivity to microtubule inhibitors. Moreover,
540 the genes contributing to benomyl resistance were not always among the highly
541 expressed genes in both transcriptomics and proteomics datasets, demonstrating that
542 even mild overexpression can lead to substantial phenotypes. These findings
543 underscore the importance of recognizing subtle (<2-fold) expression changes, as
544 they have the capacity for causing strong phenotypes.
545
546 Although increased α-tubulin expression appears to be a common mechanism of
547 aneuploidy-based benomyl resistance, we also find evidence for additional
548 mechanisms. First, not all of the genes that contributed to benomyl resistance have

549 known functions related to tubulin expression (Fig S7D). We identified two
550 components of the spindle position checkpoint (*MCK1*-chr. 14, *SWR1*-chr. 4),
551 implicating this checkpoint in mitigating the effects of microtubule-targeting drugs. We
552 also identified a drug exporter (*SNQ2*-chr. 4) and a microtubule stabilizer (*BIM1*-chr.
553 5). Importantly, the genes that we identified for resistant chromosome regions were
554 not always the most obvious candidates (Fig. S7). *TOF1*-chr. 14 and *SAP1*-chr. 5 have
555 not previously been associated with microtubule functions, but both contribute to
556 benomyl resistance on their respective aneuploid chromosomes. Second, not all of
557 the resistant disomic strains had increased α-tubulin expression (e.g. Dis14, Figure
558 3C). Third, not every region of a disomic chromosome that contributes to benomyl
559 resistance increases α-tubulin expression (Fig. S6B). Finally, we find that disomy
560 combinations with exceptionally high benomyl resistance do not increase α-tubulin
561 levels further than the single disomies (Fig. S9A). We conclude that different regions
562 on individual chromosomes can combine for beneficial aneuploidy phenotypes
563 through additive or synergistic effects from combining multiple resistance pathways.
564 Additionally, genes that we would have expected to contribute to benomyl resistance
565 based on previous knockout screens often did not have an effect when heterozygously
566 deleted from the disomic strains. The most prominent example being a drug efflux
567 pump located on chromosome 2, Flr1, which did not contribute to benomyl resistance
568 for that chromosome. Deletion of *FLR1* leads to strong benomyl sensitivity (Brôco et
569 al. 1999), yet an extra copy from the disomic chromosome did not affect resistance
570 (Fig S7A). Together, these results demonstrate that gene functions determined
571 primarily via loss-of-function mutants may often not correspond with the phenotypes
572 that emerge from increased gene expression due to copy number gain.
573
574 While mild overexpression of specific genes can confer drug resistance, the
575 overexpression of many genes across an entire chromosome greatly increases
576 aneuploidy-induced cellular stress (Torres et al. 2007; Sheltzer et al. 2011; Oromendia
577 et al. 2012; Thorburn et al. 2013; Beach et al. 2017; Li and Zhu 2022). This stress
578 presents potential targets to selectively eliminate aneuploid cells (Cohen-Sharir et al.
579 2021; Ippolito et al. 2024). However, the potential to leverage aneuploidy-based
580 sensitivities requires a deeper understanding of the underlying mechanisms driving
581 these vulnerabilities. 78% of the strains in the chromosome gain collection were
582 sensitive to hygromycin B and 66% were sensitive to heat stress (Fig. S2C). These

583 results provide additional support for decreased ribosome function and proteotoxic
584 stress as hallmarks of aneuploidy (Oromendia et al. 2012; Terhorst et al. 2020). By
585 contrast, inducing DNA damage via MMS did not result in large scale sensitivity,
586 suggesting aneuploidy-induced genome instability may be more chromosome specific.
587 Despite the general sensitivity to hygromycin, we identified a few strong examples of
588 aneuploidy-driven hygromycin resistance. Additionally, sensitivity of one chromosome
589 arm can be masked by resistance of the other arm (Fig. 5C, Fig. S4B, C). Together,
590 these results demonstrate that regions of the genome that contribute to sensitivity or
591 resistance can fully or partially counteract each other. Sensitivity and negative
592 selection have been predicted to be strong drivers of cancer karyotype evolution,
593 potentially even more so than positive selection (Jubran et al. 2024).
594
595 Given the high prevalence of aneuploidy in cancer, it is an attractive target for
596 identifying exploitable vulnerabilities. This requires a better understanding of the
597 positive and negative forces underlying aneuploid chromosome selection. This work
598 highlights additional challenges for identifying the genes responsible for aneuploidy
599 phenotypes, as they are likely to result from the combined effects of multiple genes.
600

601 **Material and methods**

602 *Yeast strains and media*

603 All yeast strains and plasmids used in this study are listed in Table S2, S3. All yeast
604 strains are derivatives of BY4741 and BY4742. All yeast strains were cultured in
605 complete synthetic media (CMS) lacking histidine, uracil, lysine, and leucine and
606 cultured at 30 °C, unless otherwise stated. For 5-FOA (Chempur, Karlsruhe, Germany,
607 220141- 70-8) selection, a concentration of 1 mg/mL was used. Growth assays were
608 always conducted in yeast extract/peptone containing 40 µg/ml adenine-HCl (YPA)
609 and 2% glucose (YPAD) in liquid cultures and plate-based assays. For high-throughput
610 drug resistance screens, 17.5 µg/ml benomyl (Sigma-Aldrich), 40 µg/ml hygromycin B
611 (Carl Roth), 0.02 % MMS (Sigma-Aldrich) or 5 nM rapamycin (Santa Cruz
612 Biotechnology) were added to YPAD agar plates. YPAD + DMSO agar plates were
613 used as controls for drugs dissolved in DMSO. Genetic manipulations such as
614 insertions and gene deletions were conducted as previously described (Longtine et al.
615 1998). Strains inducible for aneuploidy were generated using a conditional
616 centromere, as described in Anders et al. (2009). Single disomies and double disomies
617 were engineered as described in (Ravichandran et al. 2018). Each disomy was
618 generated independently with two different pairs of auxotrophic markers (*URA3* and
619 *HIS3*; *LYS2* and *LEU2*). For engineering monosomies, one copy of the endogenous
620 centromere was replaced by P_{GAL1}-*CEN3 URA3*. Flow cytometry of selected strains
621 was used to detect potential changes in ploidy and exclude strains that spontaneously
622 diploidized.

623

624 *PCR-mediated partial chromosome deletions*

625 PCR-mediated partial chromosome deletions were implemented as described in
626 Linder et al. (2017). To generate a deletion, a 500-800 bp fragment homologous to the
627 intended cut-site was combined with a resistance marker (*kanMX* or *hphNT1*) and a
628 telomeric seed sequence. The telomeric seed sequence (6x 5'CCCCAA3') was added
629 at the 3' end of the primer binding the resistance cassette. The homology sequence
630 was PCR amplified from genomic DNA with an added 30 bp homology sequence to
631 the resistance cassette. Fragments were combined using overlap extension PCR.

632 *High-throughput growth measurements*

633 For monosomies, chromosome missegregation was induced immediately before
634 plating. Strains were grown for 18h in 2 ml deep-well plates in 200 µl YPAD at 30 °C
635 (shaking). 4 µl were transferred to 150 µl of YPA plus 1% raffinose (YPAR) and grown
636 to log phase (~4h). 50 µl of YPA medium containing 4% galactose were added and
637 grown for 3h to induce chromosome missegregation. Samples were plated on 5-FOA
638 agar plates using a ROTOR HDA robot for high-throughput plating (Singer
639 Instruments, Roadwater, UK). Images were taken after 24, 48 and 72h. The
640 chromosome gain collection was grown in 2 ml deep-well plates in 200 µl CSM lacking
641 histidine, uracil, leucine and lysine at 30 °C. After 18h, cultures were diluted 1:10 in
642 1 × PBS and plated with the ROTOR HDA onto condition specific YPAD plates. Strains
643 were grown at 30 °C (if not indicated otherwise) and images were taken at different
644 time points from 24 to 72 h. Timepoints were selected for quantification based on the
645 highest resolution of growth differences between strains.
646

647 *Doubling time measurements*

648 Overnight cultures were grown in CSM lacking histidine, uracil, leucine and lysine,
649 diluted in YPAD and grown for 4h to mid log-phase. Cultures were diluted to an
650 optical density at 600 nm of 0.02 in 200 µl YPAD in 96-well plates. OD
651 measurements were taken every 15 min for 24 h using a Synergy S1 plate reader
652 (BioTek Instruments, Inc., Luzern, Switzerland).

653

654 *Serial dilutions*

655 Strains were grown over night in CSM lacking histidine, uracil, leucine and lysine.
656 Cultures were diluted in fresh media (OD ~ 0.05) and grown to log phase (OD
657 ~0.45), normalized by OD, diluted in 1 x PBS (1 : 10) and plated on condition specific
658 agar plates.
659

660 *High-throughput growth assay quantification and analysis*

661 Images of yeast colonies on plates were quantified using ImageJ (National Institute of
662 Health). Integrated densities of each spot area and surrounding area were quantified.

663 Background subtraction was done for each spot area individually by subtracting the
664 surrounding intensity from the colony intensity (Supplemental data file). For comparing
665 growth of chromosome loss strains to chromosome gain strains, 10 representative
666 chromosome loss strains were spotted on YPAD after selection on 5-FOA plates and
667 measured for colony intensity. These values were then used to adjust the growth
668 measurements for the other chromosome loss strains. Growth rate prediction of
669 double disomies and double monosomies in high throughput experiments was
670 predicted by multiplying the growth of the two individual single disomies/monosomies.
671 Epistasis scores were calculated by subtracting predicted growth from measured
672 growth. This was done for each treatment individually. Determination of genetic
673 interactions between disomic chromosomes on high drug concentrations were
674 calculated from dilution series (Fig 6A and C) by adding the measurements of the
675 individual single disomies (DisA + DisB - 1). Growth rates greater/smaller than additive
676 prediction +/- 30% were classified as synergistic genetic interaction. The same method
677 was used to identify genetic interactions between chromosome arms.
678

679 *qPCR*

680 For DNA extraction, cells were taken from plates and lysed in 20 µl of 0.02 M NaOH
681 for 10 min at 100 °C. Lysates were centrifuged for 10 min on a mini-centrifuge (Thermo
682 Fisher Scientific) to pellet cellular debris. Each 20 µl reaction contained 10 µl of Luna
683 qPCR Mastermix (New England BioLabs Inc.), 1 µl of lysate and 140 nM of each
684 primer. Measurements were made on a RealPlex2 qPCR machine (Eppendorf).
685 Cycling conditions were: activation/denaturation for 5 min at 95 °C followed by
686 40 cycles of 15 sec at 95 °C, 1 min at 60 °C with a subsequent fluorescence
687 measurement. Melting curves were generated to determine primer specificity. *Ct*
688 values were determined using the automatic thresholding of the RealPlex2 software.
689 Chromosome copy numbers were calculated using a slightly modified ΔΔCt method
690 (Schmittgen 2001). The Ct values from duplicates were averaged and used to obtain
691 the ΔCt, which was raised to the negative power of 2 to give the fold change. The ratio
692 of fold change of the test strains to that of a wild-type strain was calculated to obtain
693 the chromosome copy numbers. Karyotyping primers are in Table S5.
694

695 *Protein extraction and Western blotting*

696 For protein extraction, saturated ON cultures were diluted to an OD of 0.02 into YPAD.
697 Cells were grown to an OD of ~0.6, normalized by OD and harvested. Proteins were
698 extracted by pelleting cells, resuspending them in 100 µl ddH_2O, adding 100 µl 0.2 M
699 NaOH and incubating them at room temperature for 5 min. Cells were pelleted and
700 resuspended in 1x sample buffer before incubating them at 95° C for 3 min. Samples
701 were stored at -20°C. Membranes were stained with 0.1 % Ponceau S (Sigma Aldrich)
702 in 5% acetic acid. Total protein amount was detected with the ChemiDocMP imaging
703 system (Bio-Rad). Membranes were washed for 30 min in Tris-buffered saline with
704 0.01% Tween (TBS-T) with three buffer exchanges, blocked for 1 h in 5% BSA (Sigma-
705 Aldrich) or 5% skim milk (Gerbu Biotechnik GmbH) in TBS-T, depending on the primary
706 antibody (see below). Primary antibodies diluted in their respective blocking buffers
707 were incubated overnight at 4°C on an orbital shaker. Membranes were washed for
708 30 min in TBS-T with three buffer exchanges before and after secondary antibody
709 incubation. Horseradish peroxidase (HRP)-conjugated antimouse IgG secondary
710 antibody (1:10,000; Cell Signaling Technology 7076) diluted in the respective blocking
711 buffers was incubated for 1 h at room temperature. Chemiluminescence was
712 developed using the Amersham ECL Prime detection reagent (Cytiva) and detected
713 with the ChemiDocMP. Protein bands were quantified using ImageJ and normalized
714 to the total protein amount quantified from the Ponceau S staining. The following
715 primary antibodies were used: mouse anti-Pgk1 (in BSA and skim milk–TBST,
716 respectively; 1:20.000; Thermo Fisher Scientific 22C5D8), anti-α-Tubulin (in skim
717 milk–TBS; 1:20,000; mouse; Sigma-Aldrich T6074), anti-β-Tubulin (in BSA; 1:5.000;
718 mouse; Developmental Studies Hybridoma Bank E7).
719

720 *Flow Cytometry*

721 Cultures were grown to log-phase, pelleted and resuspended in 300 µl H_2O. 700 µl of
722 100 % EtOH were added during vertexing, and cells were fixed for 1h at room
723 temperature. Cells were pelleted and resuspended in 50 mM sodium citrate, sonicated
724 to disperse cell clumps and treated with 250 µg/mL RNase A (Sigma-Aldrich, R6513)
725 and 1 mg/mL Proteinase K (Sigma-Aldrich, P2308) overnight at 37°C. Cells were
726 resuspended in 50 mM sodium citrate solution containing 1 µM SYTOX green (Thermo
727 Fisher, 10768273). Samples were run on BD LSRFortessa Cell Analyzer equipped

728 with a 15-mW 488-nm laser. Maximum count peaks for fluorescence intensities were
729 calculated using the BD FACSDiva 8.0.1 software.
730
731 *Gene ontology enrichment analysis*
732 For GO enrichment tests, the GOrilla gene ontology tool (http://cbl-gorilla.cs.
733 technion.ac.il, accessed in September 2025) was used. The target gene list was
734 composed of all genes identified as resistance genes, and the background list was all
735 6,002 genes annotated in the *S. cerevisiae* genome. All lists of candidate genes were
736 assembled from the Saccharomyces Genome Database, based on specific phenotype
737 annotations. The list of Benomyl-related genes was based on the following
738 classifications after benomyl treatment: resistance to chemicals: decreased;
739 chromosome/plasmid maintenance: decreased; viability: decreased. 799 genes
740 contain at least one of these terms. The list of CIN-related genes was assembled using
741 the following GO terms: colony sectoring: increased; chromosome segregation:
742 abnormal; chromosome/plasmid maintenance: decreased rate; chromosome/plasmid
743 maintenance: abnormal; chromosome segregation (Clarke et al. 2023). 718 different
744 genes contain at least one of these terms. The list of tubulin/microtubule related genes
745 was based on: cytoplasmic microtubule organization; gammatubulin binding; microtubule
746 cytoskeleton organization; microtubule depolymerization; microtubule nucleation;
747 microtubule polymerization; microtubule based process; mitotic spindle assembly; mitotic
748 spindle elongation; tubulin binding; tubulin complex; tubulin complex assembly. 43 genes
749 contain at least one of these terms.
750
751 *RNA expression and protein abundance analysis*
752 Data sets from Torres et al. 2007, Dephoure et al 2014 and Muenzner et al. 2024 were
753 used to analyze RNA and protein levels. Due to the high protein sequence homology
754 between Tub1 and Tub3 (>90% identical), their protein levels where added together.
755 Expression data from Muenzner et al. was excluded from the analysis of benomyl
756 resistance driver genes, as only 4 out of 9 proteins were identified in their data set.
757
758 *Statistical analysis*
759 Statistical analysis was performed using GraphPad Prism software. Details for the
760 statistical tests used in a particular experiment are reported in the figure legends.

Competing interest statement

The authors declare no competing interests.

Acknowledgements

The authors thank the Campbell and Dammermann laboratories for helpful discussions and comments. We thank the Kraft lab and Kirk Anders for gifts of strains and plasmids and Alexander Dammermann and Sean Montgomery for careful reading of the manuscript. We acknowledge the service of the FACS Facility.

This work was supported by a Max Perutz Labs Fellowship to M.S.K and the Austrian Science Fund (FWF) grant F 8802-B to C.S.C.

Author Contributions

M.S.K conducted the majority of the experiments. M.S.K., S.F., M.C.R and C.H., generated the chromosome gain collection. C.H. and S.F. generated the chromosome loss collection. C.H. performed growth measurements and analysis of the chromosome loss collection. M.S.K. and C.S.C conceptualized the research, analyzed the data, and wrote the manuscript. All authors reviewed and approved the manuscript.

References

Adell MAY, Klockner TC, Höfler R, Wallner L, Schmid J, Markovic A, Martyniak A, Campbell CS. 2023. Adaptation to spindle assembly checkpoint inhibition through the selection of specific aneuploidies. *Genes Dev* **37**: 171–190.

Anders KR, Kudrna JR, Keller KE, Kinghorn BAA, Miller EM, Pauw D, Peck AT, Shellooe CE, Strong IJT. 2009. A strategy for constructing aneuploid yeast strains by transient nondisjunction of a target chromosome. *BMC Genet* **10**: 1–11.

Barney JB, Chandrashekarappa DG, Soncini SR, Schmidt MC. 2021. Drug resistance in diploid yeast is acquired through dominant alleles, haploinsufficiency, gene duplication and aneuploidy ed. A.M. Dudley. *PLOS Genet* **17**: e1009800.

Beach RR, Ricci-Tam C, Brennan CM, Moomau CA, Hsu P, Hua B, Silberman RE, Springer M, Amon A. 2017. Aneuploidy Causes Non-genetic Individuality. *Cell* **169**: 229-242.e21.

Beaupere C, Dinatto L, Wasko BM, Chen RB, VanValkenburg L, Kiflezghi MG, Lee MB, Promislow DEL, Dang W, Kaeberlein M, et al. 2018. Genetic screen identifies adaptive aneuploidy as a key mediator of ER stress resistance in yeast. *Proc Natl Acad Sci* **115**: 9586–9591.

Bonney ME, Moriya H, Amon A. 2015. Aneuploid proliferation defects in yeast are not driven by copy number changes of a few dosage-sensitive genes. *Genes Dev* **29**: 898–903.

Brôco N, Tenreiro S, Viegas CA, Sá-Correia I. 1999. FLR1 gene (ORF YBR008c) is required for benomyl and methotrexate resistance inSaccharomyces cerevisiae and its benomyl-induced expression is dependent on Pdr3 transcriptional regulator. *Yeast* **15**: 1595–1608.

Caydasi AK, Khmelinskii A, Darieva Z, Kurtulmus B, Knop M, Pereira G. 2023. SWR1 chromatin remodeling complex prevents mitotic slippage during spindle position checkpoint arrest ed. K. Bloom. *Mol Biol Cell* **34**: ar11.

Chen G, Bradford WD, Seidel CW, Li R. 2012. Hsp90 stress potentiates rapid cellular adaptation through induction of aneuploidy. *Nature* **482**: 246–250.

Clarke MN, Marsoner T, Adell MAY, Ravichandran MC, Campbell CS. 2023. Adaptation to high rates of chromosomal instability and aneuploidy through multiple pathways in budding yeast. *EMBO J* **42**: e111500.

Cohen-Sharir Y, McFarland JM, Abdusamad M, Marquis C, Bernhard SV, Kazachkova M, Tang H, Ippolito MR, Laue K, Zerbib J, et al. 2021. Aneuploidy renders cancer cells vulnerable to mitotic checkpoint inhibition. *Nature* **590**: 486–491.

818 Dephoure N, Hwang S, O'Sullivan C, Dodgson SE, Gygi SP, Amon A, Torres EM.
819 2014. Quantitative proteomic analysis reveals posttranslational responses to
820 aneuploidy in yeast. *eLife* **3**: e03023.

821 Garribba L, De Feudis G, Martis V, Galli M, Dumont M, Eliezer Y, Wardenaar R,
822 Ippolito MR, Iyer DR, Tijhuis AE, et al. 2023. Short-term molecular
823 consequences of chromosome mis-segregation for genome stability. *Nat*
824 *Commun* **14**: 1353.

825 Girish V, Lakhani AA, Thompson SL, Scaduto CM, Brown LM, Hagenson RA,
826 Sausville EL, Mendelson BE, Kandikuppa PK, Lukow DA, et al. 2023.
827 Oncogene-like addiction to aneuploidy in human cancers. *Science* **381**:
828 eadg4521.

829 Gresham D, Desai MM, Tucker CM, Jenq HT, Pai DA, Ward A, DeSevo CG, Botstein
830 D, Dunham MJ. 2008. The Repertoire and Dynamics of Evolutionary
831 Adaptations to Controlled Nutrient-Limited Environments in Yeast ed. M.
832 Snyder. *PLoS Genet* **4**: e1000303.

833 Hintzen DC, Soto M, Schubert M, Bakker B, Spierings DCJ, Szuhai K, Lansdorp PM,
834 Kluin RJC, Foijer F, Medema RH, et al. 2022. The impact of monosomies,
835 trisomies and segmental aneuploidies on chromosomal stability ed. D. Cimini.
836 *PLOS ONE* **17**: e0268579.

837 Hose J, Escalante LE, Clowers KJ, Dutcher HA, Robinson D, Bouriakov V, Coon JJ,
838 Shishkova E, Gasch AP. 2020. The genetic basis of aneuploidy tolerance in
839 wild yeast. *eLife* **9**.

840 Hwang S, Cavaliere P, Li R, Zhu LJ, Dephoure N, Torres EM. 2021. Consequences
841 of aneuploidy in human fibroblasts with trisomy 21. *Proc Natl Acad Sci* **118**:
842 e2014723118.

843 Ippolito MR, Martis V, Martin S, Tijhuis AE, Hong C, Wardenaar R, Dumont M, Zerbib
844 J, Spierings DCJ, Fachinetti D, et al. 2021. Gene copy-number changes and
845 chromosomal instability induced by aneuploidy confer resistance to
846 chemotherapy. *Dev Cell* **56**: 2440-2454.e6.

847 Ippolito MR, Zerbib J, Eliezer Y, Reuveni E, Viganò S, Taglietti S, Scorzoni S,
848 Gianotti S, Martin S, Muenzner J, et al. 2024. Increased RNA and protein
849 degradation is required for counteracting transcriptional burden and
850 proteotoxic stress in human aneuploid cells. *Cancer Discov* **14**.

851 Jubran J, Slutsky R, Rozenblum N, Rokach L, Ben-David U, Yeger-Lotem E. 2024.
852 Machine-learning analysis reveals an important role for negative selection in
853 shaping cancer aneuploidy landscapes. *Genome Biol* **25**: 95.

854 Kaboli S, Miyamoto T, Sunada K, Sasano Y, Sugiyama M, Harashima S. 2016.
855 Improved stress resistance and ethanol production by segmental
856 haploidization of the diploid genome in Saccharomyces cerevisiae. *J Biosci*
857 *Bioeng* **121**: 638–644.

858 Klockner TC, Campbell CS. 2024. Selection forces underlying aneuploidy patterns in
859 cancer. *Mol Cell Oncol* **11**: 2369388.

860 Li R, Zhu J. 2022. Effects of aneuploidy on cell behaviour and function. *Nat Rev Mol*
861 *Cell Biol* **23**: 250–265.

862 Linder RA, Greco JP, Seidl F, Matsui T, Ehrenreich IM. 2017. The Stress-Inducible
863 Peroxidase *TSA2* Underlies a Conditionally Beneficial Chromosomal
864 Duplication in *Saccharomyces cerevisiae*. *G3 GenesGenomesGenetics* **7**:
865 3177–3184.

866 Liu X, Wang X, Yang X, Liu S, Jiang L, Qu Y, Hu L, Ouyang Q, Tang C. 2015.
867 Reliable cell cycle commitment in budding yeast is ensured by signal
868 integration. *eLife* **4**: e03977.

869 Loegler V, Friedrich A, Schacherer J. 2024. Overview of the *Saccharomyces*
870 *cerevisiae* population structure through the lens of 3,034 genomes ed. G.
871 Brown. *G3 Genes Genomes Genet* jkae245.

872 Longtine MS, McKenzie A, Demarini DJ, Shah NG, Wach A, Brachat A, Philippsen P,
873 Pringle JR. 1998. Additional modules for versatile and economical PCR-based
874 gene deletion and modification in Saccharomyces cerevisiae. *Yeast*
875 *Chichester Engl* **14**: 953–61.

876 Lukow DA, Sausville EL, Suri P, Chunduri NK, Wieland A, Leu J, Smith JC, Girish V,
877 Kumar AA, Kendall J, et al. 2021. Chromosomal instability accelerates the
878 evolution of resistance to anti-cancer therapies. *Dev Cell* **56**: 2427-2439.e4.

879 Macaluso F, Bos T, Chiroli E, Bonaiuti P, Apuan JC, Gross F, Pompei S, Rice LM,
880 Ciliberto A. 2025. Evolutionary adaptation to hyperstable microtubules
881 selectively targets tubulins and is empowered by the spindle assembly
882 checkpoint. *Cell Rep* **44**: 115323.

883 Morard M, Macías LG, Adam AC, Lairón-Peris M, Pérez-Torrado R, Toft C, Barrio E.
884 2019. Aneuploidy and Ethanol Tolerance in Saccharomyces cerevisiae. *Front*
885 *Genet* **10**: 82.

886 Muenzner J, Trébulle P, Agostini F, Zauber H, Messner CB, Steger M, Kilian C, Lau
887 K, Barthel N, Lehmann A, et al. 2024. Natural proteome diversity links
888 aneuploidy tolerance to protein turnover. *Nature* **630**: 149–157.

889 Oromendia AB, Dodgson SE, Amon A. 2012. Aneuploidy causes proteotoxic stress in
890 yeast. *Genes Dev* **26**: 2696–2708.

891 Ozery-Flato M, Linhart C, Trakhtenbrot L, Izraeli S, Shamir R. 2011. Large-scale
892 analysis of chromosomal aberrations in cancer karyotypes reveals two distinct
893 paths to aneuploidy. *Genome Biol* **12**: R61.

894 Pan X, Yuan DS, Xiang D, Wang X, Sookhai-Mahadeo S, Bader JS, Hieter P,
895 Spencer F, Boeke JD. 2004. A Robust Toolkit for Functional Profiling of the
896 Yeast Genome. *Mol Cell* **16**: 487–496.

Passerini V, Ozeri-Galai E, de Pagter MS, Donnelly N, Schmalbrock S, Kloosterman WP, Kerem B, Storchova Z. 2016. The presence of extra chromosomes leads to genomic instability. *Nat Commun* **7**: 10754.

Pavani M, Bonaiuti P, Chiroli E, Gross F, Natali F, Macaluso F, Póti Á, Pasqualato S, Farkas Z, Pompei S, et al. 2021. Epistasis, aneuploidy, and functional mutations underlie evolution of resistance to induced microtubule depolymerization. *EMBO J* **40**: e108225.

Pavelka N, Rancati G, Zhu J, Bradford WD, Saraf A, Florens L, Sanderson BW, Hattem GL, Li R. 2010. Aneuploidy confers quantitative proteome changes and phenotypic variation in budding yeast. *Nature* **468**: 321–325.

Peter J, De Chiara M, Friedrich A, Yue J-X, Pflieger D, Bergström A, Sigwalt A, Barre B, Freel K, Llored A, et al. 2018. Genome evolution across 1,011 Saccharomyces cerevisiae isolates. *Nature* **556**: 339–344.

Rancati G, Pavelka N, Fleharty B, Noll A, Trimble R, Walton K, Perera A, Staehling-Hampton K, Seidel CW, Li R. 2008. Aneuploidy Underlies Rapid Adaptive Evolution of Yeast Cells Deprived of a Conserved Cytokinesis Motor. *Cell* **135**: 879–893.

Rathi S, Polat I, Pereira G. 2022. The budding yeast GSK-3 homologue Mck1 is an essential component of the spindle position checkpoint. *Open Biol* **12**: 220203.

Ravichandran MC, Fink S, Clarke MN, Hofer FC, Campbell CS. 2018. Genetic interactions between specific chromosome copy number alterations dictate complex aneuploidy patterns. *Genes Dev* **32**: 1485–1498.

Rojas J, Hose J, Dutcher HA, Place M, Wolters JF, Hittinger CT, Gasch AP. 2024. Comparative modeling reveals the molecular determinants of aneuploidy fitness cost in a wild yeast model. *Cell Genomics* **4**: 100656.

Ryu H-Y, Wilson NR, Mehta S, Hwang SS, Hochstrasser M. 2016. Loss of the SUMO protease Ulp2 triggers a specific multichromosome aneuploidy. *Genes Dev* **30**: 1881–1894.

Santaguida S, Vasile E, White E, Amon A. 2015. Aneuploidy-induced cellular stresses limit autophagic degradation. *Genes Amp Dev* **29**: 2010–2021.

Schatz PJ, Solomon F, Botstein D. 1986. Genetically essential and nonessential alpha-tubulin genes specify functionally interchangeable proteins. *Mol Cell Biol* **6**: 3722–3733.

Schibler A, Koutelou E, Tomida J, Wilson-Pham M, Wang L, Lu Y, Cabrera AP, Chosed RJ, Li W, Li B, et al. 2016. Histone H3K4 methylation regulates deactivation of the spindle assembly checkpoint through direct binding of Mad2. *Genes Dev* **30**: 1187–1197.

Schmittgen TD. 2001. Real-Time Quantitative PCR. *Methods* **25**: 383–385.

936 Selmecki A, Forche A, Berman J. 2006. Aneuploidy and Isochromosome Formation
937 in Drug-Resistant *Candida albicans*. *Science* **313**: 367–370.

938 Selmecki AM, Dulmage K, Cowen LE, Anderson JB, Berman J. 2009. Acquisition of
939 Aneuploidy Provides Increased Fitness during the Evolution of Antifungal
940 Drug Resistance ed. H.D. Madhani. *PLoS Genet* **5**: e1000705.

941 Sheltzer JM, Blank HM, Pfau SJ, Tange Y, George BM, Humpton TJ, Brito IL,
942 Hiraoka Y, Niwa O, Amon A. 2011. Aneuploidy Drives Genomic Instability in
943 Yeast. *Science* **333**: 1026–1030.

944 Shukla A, Nguyen THM, Moka SB, Ellis JJ, Grady JP, Oey H, Cristino AS, Khanna
945 KK, Kroese DP, Krause L, et al. 2020. Chromosome arm aneuploidies shape
946 tumour evolution and drug response. *Nat Commun* **11**: 449.

947 Sousa A, Gonçalves E, Mirauta B, Ochoa D, Stegle O, Beltrao P. 2019. Multi-omics
948 Characterization of Interaction-mediated Control of Human Protein
949 Abundance levels. *Mol Cell Proteomics* **18**: S114–S125.

950 Stingele S, Stoehr G, Peplowska K, Cox J, Mann M, Storchova Z. 2012. Global
951 analysis of genome, transcriptome and proteome reveals the response to
952 aneuploidy in human cells. *Mol Syst Biol* **8**: 608.

953 Su XA, Ma D, Parsons JV, Replogle JM, Amatruda JF, Whittaker CA, Stegmaier K,
954 Amon A. 2021. *RAD21* is a driver of chromosome 8 gain in Ewing sarcoma to
955 mitigate replication stress. *Genes Dev* **35**: 556–572.

956 Sugiyama M, Ikushima S, Nakazawa T, Kaneko Y, Harashima S. 2005. PCR-
957 Mediated Repeated Chromosome Splitting in *Saccharomyces* Cerevisiae.
958 *BioTechniques* **38**: 909–914.

959 Sugiyama M, Nakazawa T, Murakami K, Sumiya T, Nakamura A, Kaneko Y,
960 Nishizawa M, Harashima S. 2008. PCR-mediated one-step deletion of
961 targeted chromosomal regions in haploid Saccharomyces cerevisiae. *Appl*
962 *Microbiol Biotechnol* **80**: 545–53.

963 Terhorst A, Sandikci A, Keller A, Whittaker CA, Dunham MJ, Amon A. 2020. The
964 environmental stress response causes ribosome loss in aneuploid yeast cells.
965 *Proc Natl Acad Sci U S A* **117**: 17031–17040.

966 Thorburn RR, Gonzalez C, Brar GA, Christen S, Carlile TM, Ingolia NT, Sauer U,
967 Weissman JS, Amon A. 2013. Aneuploid yeast strains exhibit defects in cell
968 growth and passage through START ed. D.J. Lew. *Mol Biol Cell* **24**: 1274–
969 1289.

970 Tong AHY, Lesage G, Bader GD, Ding H, Xu H, Xin X, Young J, Berriz GF, Brost RL,
971 Chang M, et al. 2004. Global Mapping of the Yeast Genetic Interaction
972 Network. *Science* **303**: 808–813.

973 Torres EM, Sokolsky T, Tucker CM, Chan LY, Boselli M, Dunham MJ, Amon A. 2007.
974 Effects of Aneuploidy on Cellular Physiology and Cell Division in Haploid
975 Yeast. *Science* **317**: 916–924.

Trakala M, Aggarwal M, Sniffen C, Zasadil L, Carroll A, Ma D, Su XA, Wangsa D, Meyer A, Sieben CJ, et al. 2021. Clonal selection of stable aneuploidies in progenitor cells drives high-prevalence tumorigenesis. *Genes Dev* **35**: 1079–1092.

Tsai H-J, Nelliat A. 2019. A Double-Edged Sword: Aneuploidy is a Prevalent Strategy in Fungal Adaptation. *Genes* **10**: 787.

Ubeda J-M, Légaré D, Raymond F, Ouameur AA, Boisvert S, Rigault P, Corbeil J, Tremblay MJ, Olivier M, Papadopoulou B, et al. 2008. Modulation of gene expression in drug resistant Leishmania is associated with gene amplification, gene deletion and chromosome aneuploidy. *Genome Biol* **9**: R115.

Voordeckers K, Kominek J, Das A, Espinosa-Cantú A, De Maeyer D, Arslan A, Van Pee M, Van Der Zande E, Meert W, Yang Y, et al. 2015. Adaptation to High Ethanol Reveals Complex Evolutionary Pathways ed. J. Zhang. *PLOS Genet* **11**: e1005635.

Wangsa D, Braun R, Stuelten CH, Brown M, Bauer KM, Emons G, Weston LA, Hu Y, Yang HH, Vila-Casadesús M, et al. 2019. Induced Chromosomal Aneuploidy Results in Global and Consistent Deregulation of the Transcriptome of Cancer Cells. *Neoplasia* **21**: 721–729.

Watson EV, Lee JJ-K, Gulhan DC, Melloni GEM, Venev SV, Magesh RY, Frederick A, Chiba K, Wooten EC, Naxerova K, et al. 2024. Chromosome evolution screens recapitulate tissue-specific tumor aneuploidy patterns. *Nat Genet* **56**: 900–912.

Weaver BA, Cleveland DW. 2006. Does aneuploidy cause cancer? *Curr Opin Cell Biol* **18**: 658–667.

Williams BR, Prabhu VR, Hunter KE, Glazier CM, Whittaker CA, Housman DE, Amon A. 2008. Aneuploidy Affects Proliferation and Spontaneous Immortalization in Mammalian Cells. *Science* **322**: 703–709.

Yona AH, Manor YS, Herbst RH, Romano GH, Mitchell A, Kupiec M, Pilpel Y, Dahan O. 2012. Chromosomal duplication is a transient evolutionary solution to stress. *Proc Natl Acad Sci* **109**: 21010–21015.

Zerbib J, Ippolito MR, Eliezer Y, De Feudis G, Reuveni E, Savir Kadmon A, Martin S, Viganò S, Leor G, Berstler J, et al. 2024. Human aneuploid cells depend on the RAF/MEK/ERK pathway for overcoming increased DNA damage. *Nat Commun* **15**: 7772.

Zhang K, Zhang L-J, Fang Y-H, Jin X-N, Qi L, Wu X-C, Zheng D-Q. 2016. Genomic structural variation contributes to phenotypic change of industrial bioethanol yeast *Saccharomyces cerevisiae* ed. Z. Zhao. *FEMS Yeast Res* **16**: fov118.

Zhou X, Hilk A, Solis NV, Scott N, Beach A, Soisangwan N, Billings CL, Burrack LS, Filler SG, Selmecki A. 2024. Single-cell detection of copy number changes reveals dynamic mechanisms of adaptation to antifungals in Candida albicans. *Nat Microbiol* **9**: 2923–2938.

Figure 1: Strong genetic interactions between aneuploid chromosomes are rare

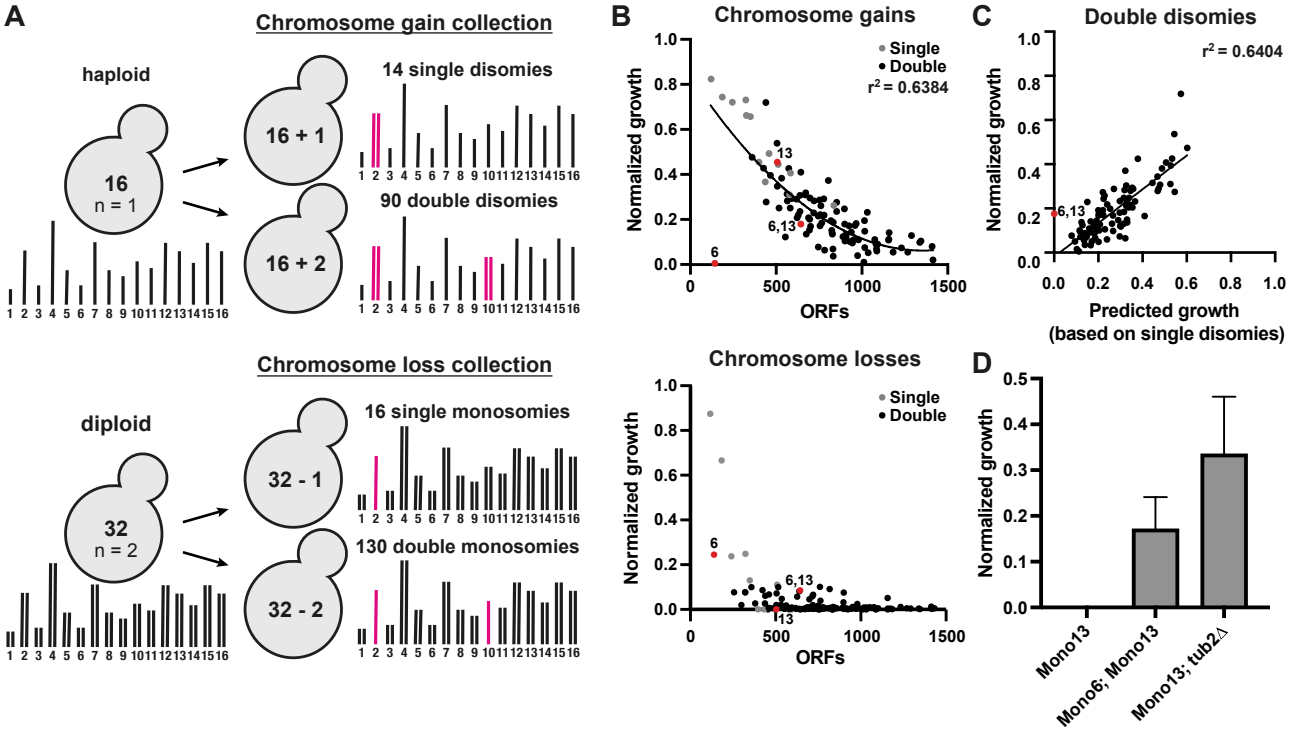

Figure 1: Strong genetic interactions between aneuploid chromosomes are rare
(A) Schematic overview of the chromosome gain and chromosome loss collections. (B) Quantified growth of the chromosome gain and chromosome loss collections. The averages of four independent high-throughput growth assays were normalized to WT. Colony intensities were quantified after 24h on YPAD plates for chromosome gains, and 72h on plates containing 5-Fluoroorotic Acid (5-FOA) for chromosome losses. Single disomies/monosomies are depicted in grey, double disomies/monosomies in black. r^2 values are from quadratic fitts. (C) Correlation between growth of the double disomies and growth predictions based on the single disomies ($p < 0.0001$). Growth was predicted by calculating the product of single disomy growth. r^2 values are from simple linear regression and p-values are from *F*-tests. (D) Quantification of colony sizes on YPAD plates after 48h normalized to a euploid diploid strain. (n=3).

Figure 2: The strongest drug resistance phenotypes come from complex aneuploidy

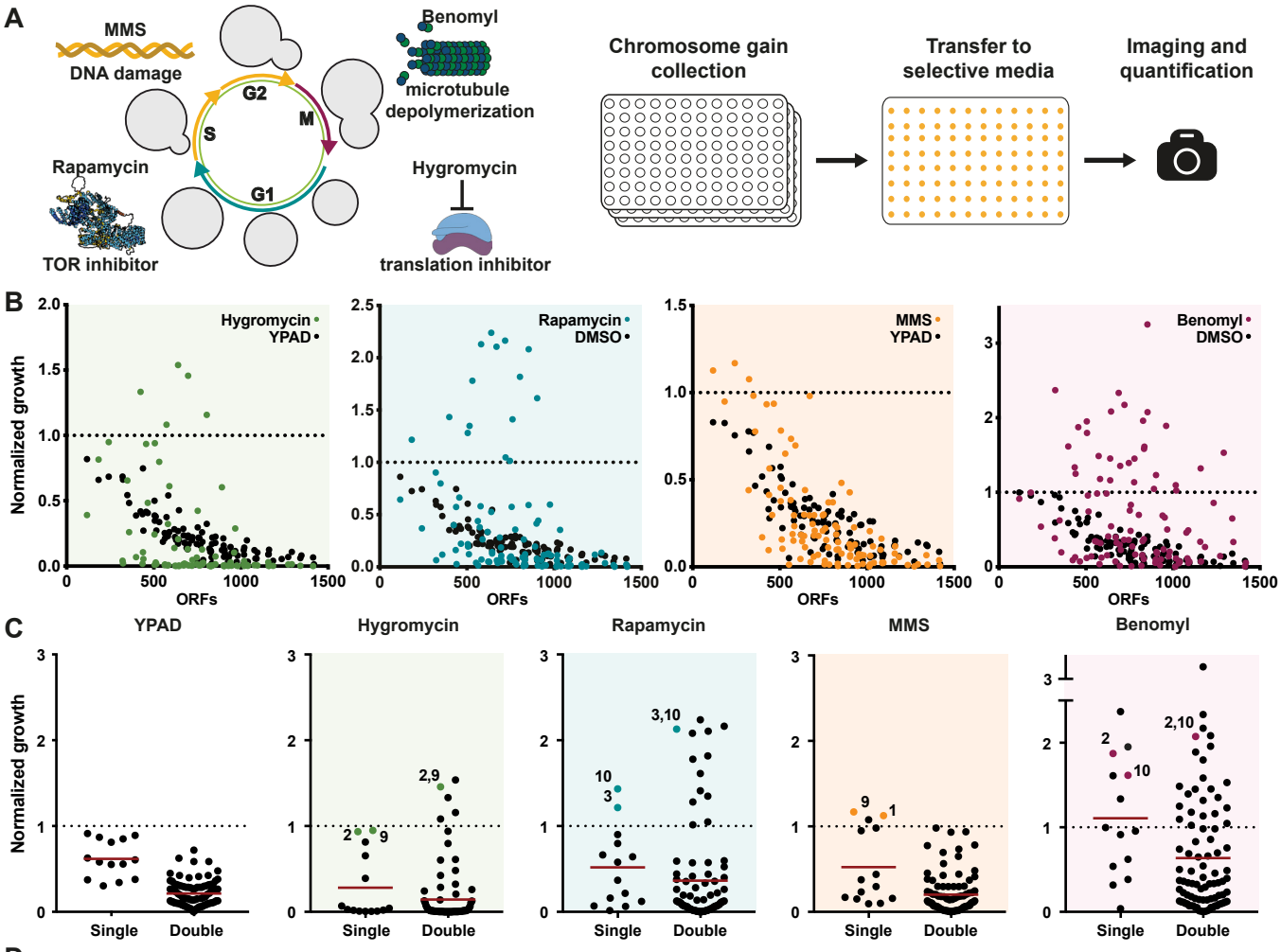

D

Genetic interactions for chromosome combinations

	YPAD	DMSO	Hygromycin	Rapamycin	MMS	Benomyl
positive	3	2	13	14	2	35
negative	2	2	0	4	7	33

Figure 2: The strongest drug resistance phenotypes come from complex aneuploidy

(A) Schematic of the work-flow for plate-based high throughput growth assays under selective conditions. Cells were grown in liquid cultures before being transferred to condition specific agar plates. Images for colony intensities were taken after 24, 36 , or 48h. (B) Averaged growth of two independent high-throughput growth assays. Control plates were quantified after 24h; hygromycin (40 µg/ml) and rapamycin (5 nM) plates after 48h; and MMS (0.02%) and benomyl (17.5 µg/ml) plates after 36h. All quantifications were normalized to a haploid WT. (C) Growth measurements of single disomies (Single) and double disomies (Double) across different treatments. Mean of each group is indicated by a red line. The YPAD control is an average of YPAD and YPAD + DMSO plate growth. The dashed line indicates WT growth. (D) Epistasis scores were calculated by subtracting the predicted growth (the product of the growth of the single disomies) from the measured growth. Genetic interactions are based on the normal distribution of epistasis scores without selective pressure. Positive genetic interactions have an epistasis score greater than the median plus 2 standard deviations and negative interactions have an epistasis score less than the median minus 2 standard deviations.

Figure 3: Benomyl resistance correlates with alpha-tubulin expression in aneuploid strains

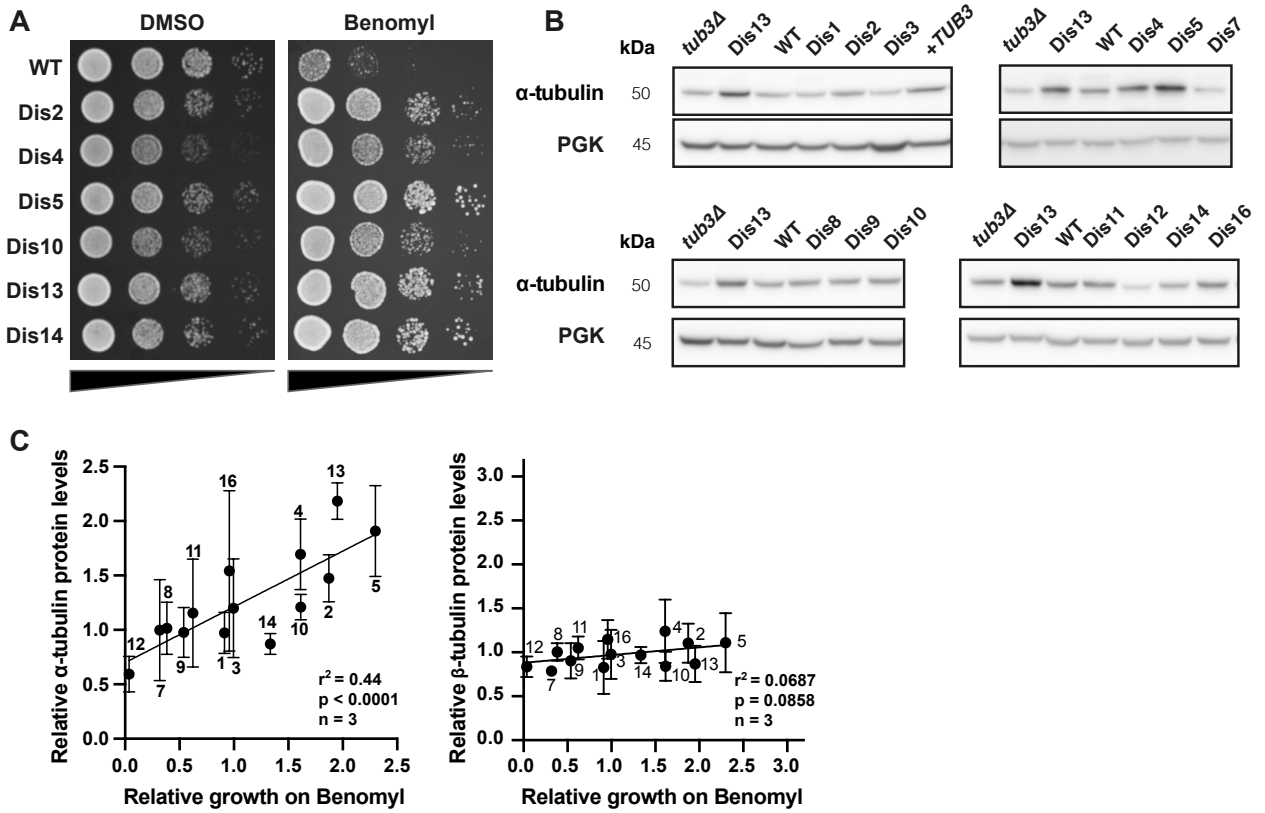

Fiure. 3: Benomyl resistance correlates with alpha-tubulin expression in aneuploid strains
(A) 10-fold serial dilution analysis of benomyl resistant single disomies on control (YPAD + DMSO, 24h) and treated (YPAD + 20 µg/ml benomyl, 48h) plates. (B) Western blot analysis of α-tubulin expression levels of single disomies. *Pgk1* is shown as a loading control. (C) Western blot quantifications of α-tubulin (n = 3) and β-tubulin (n = 3) expression levels for all single disomies. Strains were grown in YPAD and harvested in log-phase. Quantified bands were normalized to the Ponceau stained membrane and the haploid WT. Relative growth on benomyl denotes the average growth of single disomies from two independent high throughput colony size assays. r^2 values are from simple linear regression and p-values are from *F*-tests.

Figure 4: Identification of chromosome arms necessary for aneuploidy-based drug resistance

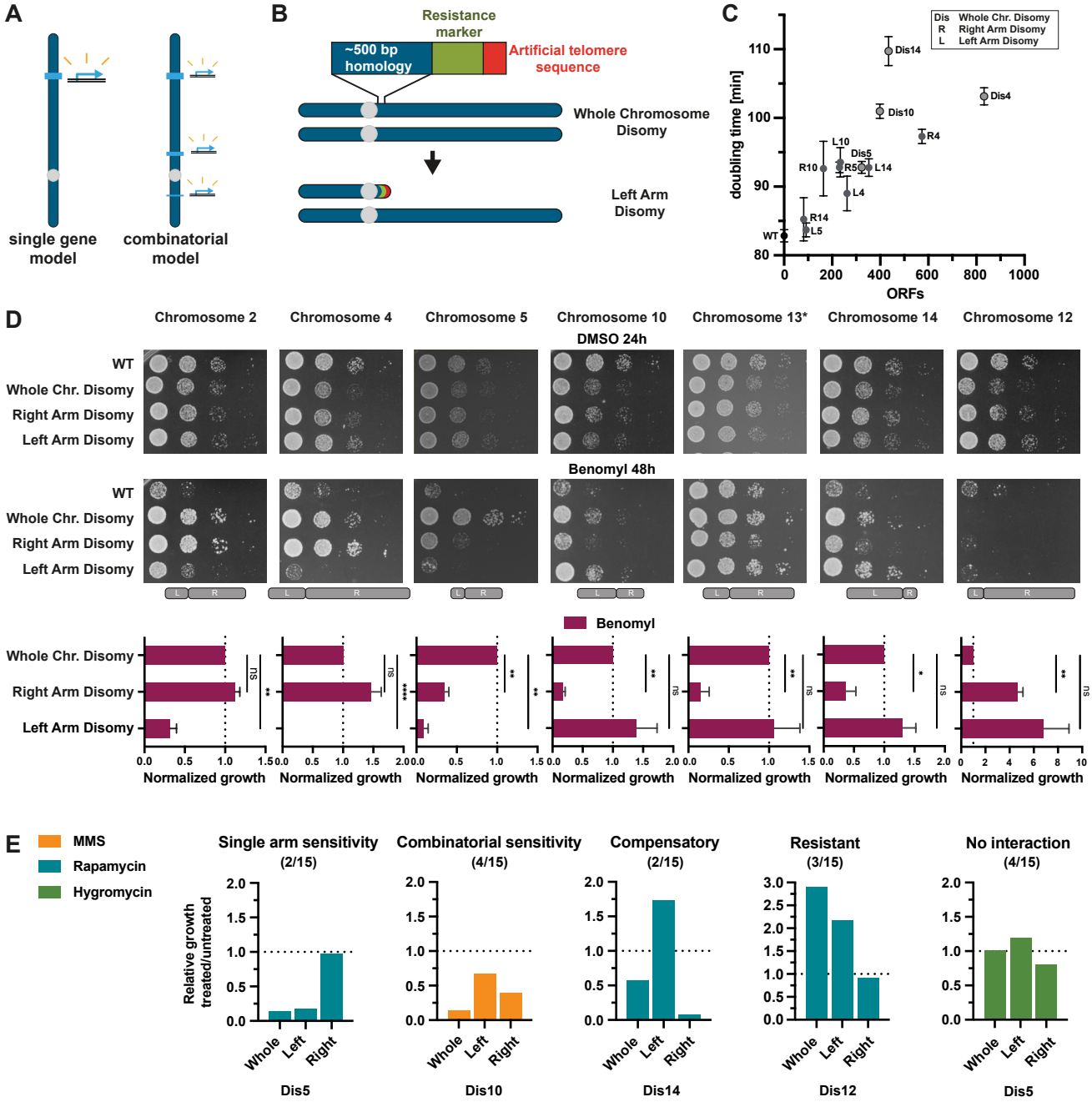

Figure 4: Identification of chromosome arms necessary for aneuploidy-based drug resistance.

(A) Schematic of two models for the genetic basis behind aneuploidy driven drug resistance. (B) Method of chromosome arm deletion. Chromosome arms are deleted by homologous recombination with a 500 bp homology sequence connected to a resistance marker and a telomeric seed sequence. (C) Doubling times of whole chromosome and single arm disomies for chromosomes 4, 5, 10 and 14. ORFs depict the remaining aneuploid ORFs after chromosome arm deletions. (D) 10-fold dilution series and quantification of whole chromosome and single arm disomies (n=3). Control plates (YPAD + DMSO) were imaged after 24h and treated plates (YPAD + 25 µg/ml benomyl) after 48h. * Indicates a lower benomyl concentration (20 µ/ml benomyl). The second dilution was quantified and normalized to WT, with the exceptions of chromosome 13 (third dilution) and chromosome 12 (first dilution). p-values are from one-way ANOVA, uncorrected Fisher's LSD test. (E) Quantification of 10-fold serial dilutions treated with MMS (0.04 %), rapamycin (10 nM) or hygromycin (60 µg/ml). Relative growth was calculated as the ratio of normalized growth on treated plates (48h) to normalized growth on control plates (24h). Representative examples for single arm sensitivity, combinatorial sensitivity, compensatory sensitivity, resistance, and no interactions are shown. Images and quantifications of all 10-fold serial dilutions are depicted in Supplemental Fig. S4A, B.

Figure 5: Most aneuploidy-based drug resistance phenotypes come from the combined effects of multiple genes.

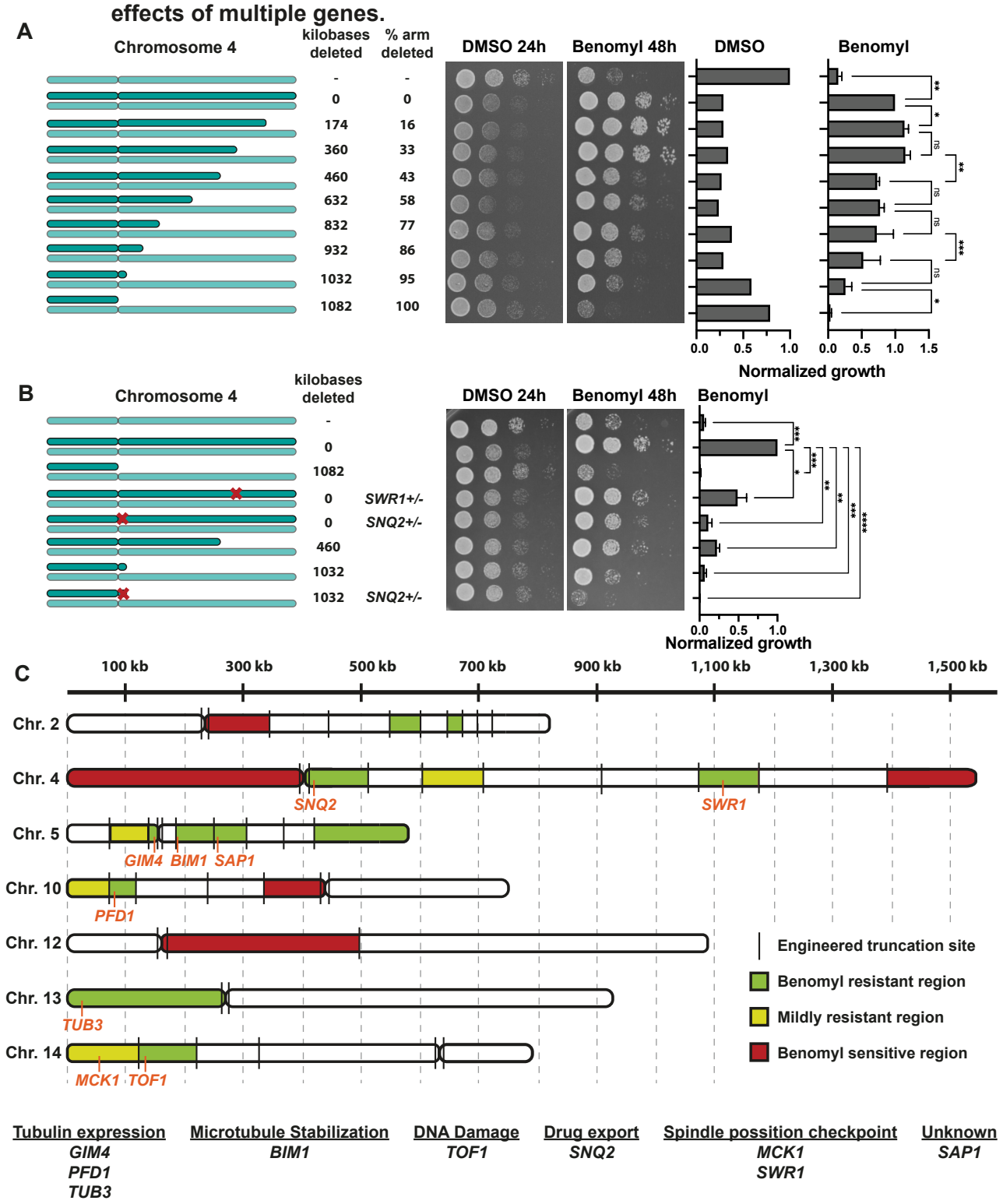

Figure 5: Most aneuploidy-based drug resistance phenotypes come from the combined effects of multiple genes.
(A) Representative image of 10-fold serial dilution and quantification of partial chromosome arm deletions of the right arm of chromosome 4. For control plates (YPAD + DMSO) the 2rd spot was quantified after 24h and for treated plates (YPAD + 25µg/ml benomyl) the 2nd and 3rd spots were quantified and averaged after 48h (n=3). p-values are from one-way ANOVA, uncorrected Fisher's LSD test. Growth on DMSO was normalized to a haploid WT and growth on benomyl to a strain disomic for chromosome 4. (B) 10-fold serial dilution and quantification of partial chromosome arm deletions and heterozygous deletions of genes contributing to benomyl resistance. For treated plates (YPAD + 25µg/l benomyl) the 3rd spot was quantified after 48h and normalized to the strain disomic for chromosome 4 (n=3). p-values are from one-way ANOVA, uncorrected Fisher's LSD test. (C) Schematic depiction of benomyl resistant and sensitive chromosome regions. Identified resistance genes are indicated in orange at their approximate chromosomal location.

Figure 6: Synergistic effects contribute to the strongest aneuploidy phenotypes.

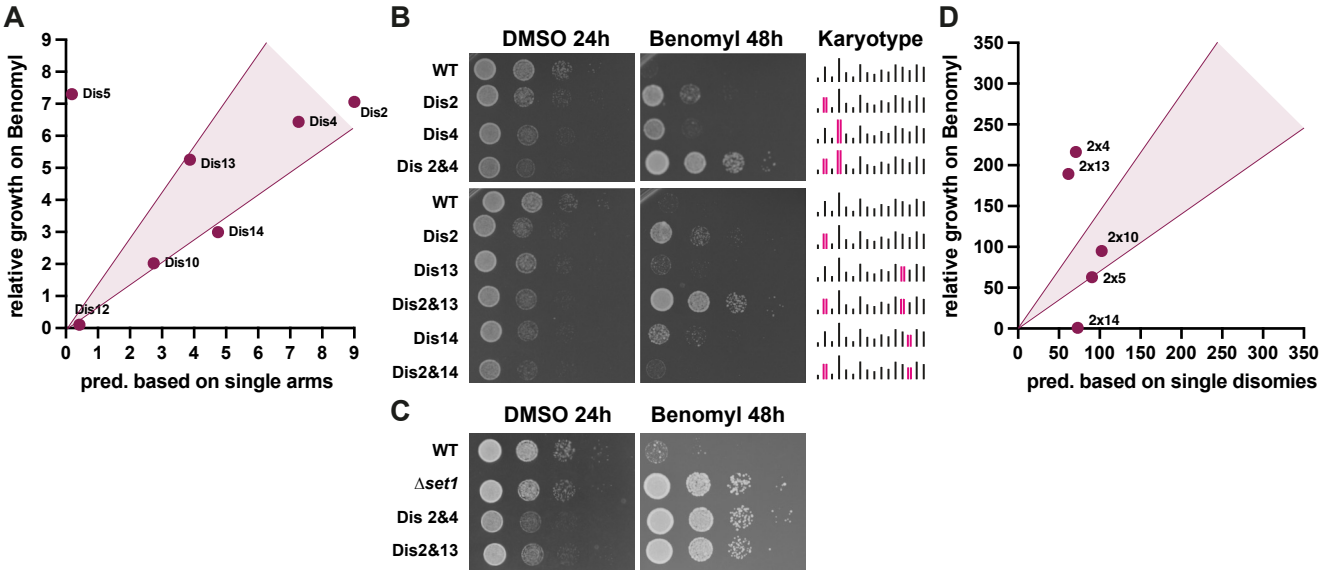

Figure 6: Synergistic effects contribute to the strongest aneuploidy phenotypes.
(A) Single disomy growth on benomyl compared to growth predictions based on single arm disomies. Growth was quantified from 10-fold serial dilutions in Figure 4D. The area highlighted in magenta indicates additive genetic interactions (+/-30% of predicted growth). Disomies that fall below this threshold are considered a negative synergistic interaction and those above are considered a positive synergistic interaction. (B) 10-fold serial dilution of single and double disomies. Control plates (YPAD + DMSO) were imaged after 24h and treated plates (YPAD + 30 µg/ml benomyl) after 48h. (C) 10-fold serial dilutions of benomyl resistant *set1*Δ haploid and two synergistically interacting double disomies (2&4, 2&13). Benomyl plates contained 30 µg/ml benomyl. (D) Quantification of the 10-fold serial dilutions of the double disomies on plates with 30 µg/ml benomyl compared to predicted growth based on the additive resistance of the single disomies (for images, see Sup. Figure 8A). Combinations in the highlighted area (magenta) are additive genetic interactions (+/-30% of predicted growth). Disomy combinations that fall below this threshold are considered a negative synergistic interaction and those above are considered a positive synergistic interaction.